Spacecraft Formation Guidance Law using a State Transition Matrix with Gravitational, Drag and Third-Body Perturbations

Yazan Chihabi* and Steve Ulrich†
Carleton University, Ottawa, Ontario, Canada, K1S5B6

There has been a growing interest in spacecraft formation-flying for space science applications. Such missions will require an accurate and efficient dynamics model, within the guidance system, to calculate and control the desired relative motion. This paper achieves an accurate analytical solution of relative motion between two spacecraft using relative classical orbital elements. The analytical solution is obtained by propagating the relative orbital elements forward in time, while taking into account gravitational field up to the fifth harmonic, third-body and drag, and calculating the relative motion in the local-vertical-local-horizontal reference frame at each time-step. Specifically, the solution proposed in this paper requires only a single matrix multiplication with the initial orbital elements and the desired time to compute the relative motion, since the solution utilized Jacobian matrices evaluated at the target spacecraft's initial orbital elements which need only be calculated once. The analytical solution was observed to accurately describe the relative motion when compared with a numerical simulator, yielding errors on the order of meters for separation distances on the order of thousands of meters. Additionally, the solution maintained accurate tracking performance when used within a back-propagation guidance law.

I. Introduction

Space science missions, such as mapping other planets and moons, require the reduction of costs and an improvement of efficiency to meet the world's growing interest [1]. Formation flying of multiple spacecraft is a vital technology for such missions as it offers lower costs and increased efficiency by reducing the mass, power demand and size of the space buses. European Space Agency's Proba-3 mission will use two spacecraft flying in formation in attempt to study the sun by creating an artificial solar eclipse [2]. However, formation flying has many considerations to be taken into account when compared to that of single spacecraft missions. The main considerations are with regards to the guidance systems, since they are responsible for calculating and controlling the desired relative motion between the spacecraft. To ensure accuracy, the guidance system must take into account perturbations since ignoring orbital perturbations in the design of the reference trajectories would result in additional propellant consumption to force the follower spacecraft to follow the reference trajectory. Furthermore, the dynamics model must be accurate for high eccentricity values, and large separation distances while remaining computationally in-expensive for on-board implementation purposes. Accurate numerical models which take into account perturbations exist; however, they are computationally expensive and can lead to errors due to integration tolerances. Therefore, an analytical dynamics model is required since it satisfies these conditions and does not require numerical integration. Formulations which take into account perturbations, such as gravitational field caused by oblateness of the earth, third body effects, and drag, exist in literature. The gravitational perturbation is particularly important when modeling orbits as it causes rotation of the line of apsides and precession of the line of nodes, along with changes in inclination and eccentricity values. In terms of the third body perturbation, it is important when modeling higher altitude orbits since it also causes rotation of the line of apsides and precession of the line of nodes. Finally, drag is important when modeling LEO (low earth orbits) since drag acts in the opposite direction to the velocity vector and hence reduces the orbital energy which in turn reduces the orbital semi-major axis and eccentricity such that the spacecraft slowly spirals down into Earth or any other planet with an atmosphere.

The most used analytical model in formation flying is the Hill-Clohessy-Wiltshire (HCW) model [3], which provides linearized relative dynamics based upon exact non-linear differential equations of motion in the LVLH (Local-vertical-local-horizontal) reference frame. The HCW model, due to the fact they are linearized equations of

*Graduate Research Assistant, Department of Mechanical and Aerospace Engineering, Carleton University, 1125 Colonel By Drive, Ottawa, ON, K1S5B6, Canada
†Associate Professor, Department of Mechanical and Aerospace Engineering, Carleton University, 1125 Colonel By Drive, Ottawa, ON, K1S5B6, Canada.

motion and time invariant, is perfect for the application of a linear state feedback controller design such as optimal feedback control method and linear quadratic regulator (LQR) method. [4] However, the model only works for circular Keplerian orbits as it does not take into account perturbations and simplifications made in the derivation causes it to be in-accurate for modeling elliptical reference orbits. When applying an eccentric reference orbit to the HCW model, the errors increase with increasing eccentricity and it has been shown that the effect neglecting eccentricity in the HCW model greatly outweighs the effect of external perturbations. [5] Furthermore, the linear-time-invariant (LTI) HCW equations were extended by Inalhan, et al. [5] to include arbitrary eccentricity by reformulating the HCW as linear-parameter-varying (LPV) which enables the use LPV control techniques, such as model predictive control. An analytical solution, which was first suggested by Hill [6] that incorporates Keplerian eccentric orbits and valid for any time-step, was formulated by Gurfil and Kholshevnikov. [7, 8] The solution uses classical orbital elements as constant parameters to calculate the relative dynamics of a chaser spacecraft, analogous to a simple rotation matrix approach, instead of cartesian initial conditions used in the HCW model. The most important advantage of using this approach is the fact that the orbital elements can be made to vary as a function of time to include the effects of orbital perturbations [9, 10]. Furthermore, Schaub extended Gurfil and Kholshevnikov's equations through linearizations such that the cartesian coordinates in the LVLH reference frame are expressed in terms of orbital element differences [11]. Another analytical solution, proposed by Mahajan, et al. [12], uses linearized state transition matrices to propagate the relative mean orbital elements forward in time while taking into account the effects of gravitation field perturbation up to an arbitrary selected degree. Additionally, Guffanti, et al. introduced a set of state transition matrices which included the effects of the second and third zonal harmonics, third body, and solar radiation pressure where non-singular orbital elements were used as the states [13].

The work presented in this paper focuses on third body effects of the sun and moon, drag and gravitational up to fifth zonal harmonic using a similar state transition matrix development technique presented by Guffanti, et al.[13] and Mahajan, et al. [12]. The third body linearized equations used were formulated by Prado [14, 15] and Kozai [16, 17] formulated linearized equations for effects of lunisolar perturbations on orbital elements, and Blitzer [18] formulated equations for drag. Furthermore, Brouwer [19], Liu [20], and Kozai [21] formulated equations for the gravitational perturbation up to fifth zonal harmonic (J_5). Specifically, this work build's upon the work of Kuiack and Ulrich [22], where they implemented linearized short periodic and secular variations of the orbital elements formulated by Brouwer for the second zonal harmonic (J_2) [19] into Gurfil and Kholshevnikov's equations of motion [7, 8]. Using this formulation, Kuiack and Ulrich implemented a back propagation technique such that a set of initial conditions for the chaser spacecraft in terms of orbital elements is found to allow the spacecraft to drift into a desired relative orbital elements [22]. The work presented in this paper aims to provide a simple, yet sophisticated method of implementing back propagation and forward propagation guidance laws. Although simpler than more sophisticated methods being developed for propagating perturbed relative motion analytically, this paper may provide a slightly different viewpoint on developing relative motion methodologies. Specifically, the methodology presented here lends itself to a relative motion viewpoint involving relative distances, or metrics, as the work is a direct continuation of the methods presented by Kuiack and Ulrich's back propagation guidance law [22]. However, one of the key differences is the state-transition matrix approach and the determination of relative orbital elements using desired Cartesian coordinates instead.

II. Linearized Equations of Relative Motion using Relative Orbital Elements

The non-linear equations of motion formulated by Gurfil and Kholshevnikov provides a method of calculating the relative motion of two spacecraft in the LVLH reference frame using each spacecraft's orbital elements. [7, 8] The LVLH reference frame is denoted by $\mathcal{F}_L$ and defined by its orthonormal unit vectors $[\vec{L}_x, \vec{L}_y, \vec{L}_z]^T$ with its origin at the target spacecraft. The unit vector $\vec{L}_z$ points in the same direction as the orbit's angular momentum vector normal to the orbital plane. $\vec{L}_x$ points in the direction of the target's inertial position $\vec{r}_t$ and $\vec{L}_y$ completing the triad such that $\vec{L}_y = \vec{L}_z \times \vec{L}_x$. However, orbital elements cannot be determined from Cartesian coordinates using these equations which means these equations cannot be used to determine relative orbital elements using a set of desired Cartesian coordinates. Therefore, a set of linearized equations that describe the relative motion must be used. Schaub derives the linearized equations of motion using a first order approximation and is presented in state-space form below [11]

$$\boldsymbol{\rho} = \begin{bmatrix} x & y & z \end{bmatrix}^T = \boldsymbol{A}_1 \Delta \boldsymbol{x} \tag{1}$$

such that $\vec{\rho} = \boldsymbol{\rho}^T \vec{\mathcal{F}}_L$ and

$$\boldsymbol{x} = \begin{bmatrix} a & e & i & \omega & \Omega & M \end{bmatrix}^T \tag{2}$$

$$\boldsymbol{A}_1 = \begin{bmatrix} \frac{r_t}{a_t} & -a_t \cos\theta_t & 0 & 0 & 0 & \frac{a_t e_t \sin\theta_t}{\sqrt{1-e_t{}^2}} \\ 0 & \frac{r_t \sin\theta_t}{1-e_t{}^2}(2 + e_t \cos\theta_t) & 0 & r_t & r_t \cos i_t & \frac{r_t}{(1-e_t{}^2)^{3/2}} \\ 0 & 0 & r_t \sin\theta_t & 0 & -r_t \cos\theta_t \sin\theta_t & 0 \end{bmatrix} \tag{3}$$

The classical orbital elements, denoted by a, e, i, ω, Ω and M represent the semi-major axis, eccentricity, inlination, argument of perigee, right ascension of the ascending node, and mean anomaly respectively. The variable $\Delta\boldsymbol{x}$ contains the difference in orbital elements between the chaser and the target spacecraft such that $\Delta\boldsymbol{x} = \boldsymbol{x}_c - \boldsymbol{x}_t$, where the subscripts c and t denote the chaser and target respectively.

Schaub also derives equations for relative velocity in the LVLH reference frame, however; they are derived in terms of non-singular orbital elements. The linearized equations relating relative orbital elements to relative velocity are herein derived by taking the time derivative of Equation (1) shown below

$$\dot{\boldsymbol{\rho}} = \begin{bmatrix} \dot{x} & \dot{y} & \dot{z} \end{bmatrix}^T = \left(\frac{d}{dt}\boldsymbol{A}_1\right)\Delta\boldsymbol{x} + \boldsymbol{A}_1 \Delta\dot{\boldsymbol{x}} \tag{4}$$

It will be shown in the following section that $\Delta\dot{\boldsymbol{x}} = \boldsymbol{F}\Delta\boldsymbol{x}$, where $\boldsymbol{F}$ contains the combined keplerian and perturbing effects. The relative velocity in LVLH can be simplified as

$$\dot{\boldsymbol{\rho}} = \left(\begin{bmatrix} \boldsymbol{A}_{21} & \boldsymbol{A}_{22} \end{bmatrix} + \boldsymbol{A}_1 \boldsymbol{F}\right)\Delta\boldsymbol{x} \tag{5}$$

where

$$\boldsymbol{A}_{21} = \begin{bmatrix} \frac{\dot{r}_t}{a_t} & a_t \dot{\theta}_t \sin\theta_t & 0 \\ 0 & \begin{matrix} \frac{1}{1-e_t{}^2}[\dot{r}_t \sin\theta_t (2 + e_t \cos\theta_t) + \\ \dot{\theta}_t \cos\theta_t r_t (2 + e_t \cos\theta_t) + \sin\theta_t r_t (2 - e_t \dot{\theta}_t \sin\theta_t)] \end{matrix} & 0 \\ 0 & 0 & \dot{r}_t \sin\theta_t + r_t \dot{\theta}_t \cos\theta_t \end{bmatrix} \tag{6}$$

$$\boldsymbol{A}_{22} = \begin{bmatrix} 0 & 0 & \frac{a_t e_t \dot{\theta}_t \cos\theta_t}{\sqrt{1-e_t{}^2}} \\ \dot{r}_t & \dot{r}_t \cos i_t & \frac{\dot{r}_t}{(1-e_t{}^2)^{3/2}} \\ 0 & -\dot{r}_t \cos\theta_t \sin\theta_t + r_t \dot{\theta}_t (\sin\theta_t + \cos\theta_t) & 0 \end{bmatrix} \tag{7}$$

The target's position, velocity and true anomaly rate magnitudes (r_t, $\dot{r}_t$, and $\dot{\theta}_t$) are calculated as follows

$$r_t = \frac{a_t(1 - e_t{}^2)}{1 + e_t \cos\theta_t} \tag{8}$$

$$\dot{r}_t = \sqrt{\frac{\mu}{a_t(1 - e_t{}^2)}} e_t \sin(\theta_t) \tag{9}$$

$$\dot{\theta}_t = \frac{\sqrt{\mu a_t (1 - e_t{}^2)}}{r_t{}^2} \tag{10}$$

where θ_t is the target's true anomaly.

Since the equations shown above are functions of the true anomaly, θ, a way of computing it is required. Gurfil and kholshevnikov [7] proposed to numerically integrate for the time derivative of the true anomaly, but the purpose of this paper is to provide a fully analytical solution. Many solutions to obtain the true anomaly from the mean anomaly, eccentric anomaly and the orbit's eccentricity exist. Vallado illustrates many of these methods, including a method that uses modified Bessel functions of the first kind paired with the eccentricity and mean anomaly to solve for the true anomaly [23]. Kuiack and Ulrich[22] modified Gurfil and Kholeshnikov's solution to include a analytical approximation for the true anomaly in terms of the eccentric anomaly. The simple recursive solution is given by

$$E = M + e \sin(M + e \sin(M + e \sin(M + \ldots + e \sin(M)))) \tag{11}$$

$$\cos\theta = \frac{\cos E - e}{1 - e\cos E} \tag{12}$$

$$\sin\theta = \frac{\sqrt{1-e^2}\sin E}{1 - e\cos E} \tag{13}$$

$$\theta = \tan^{-1}\frac{\sin\theta}{\cos\theta} \tag{14}$$

where E is the eccentric anomaly. This is a recursive solution based on the Newton-Raphson Iteration Technique* which implies an infinite series. Therefore, a term will become truncated based on the desired accuracy. The mean anomaly can be found by

$$M = M_0 + \dot{M}(t_f - t_0) \tag{15}$$

$$\dot{M} = n = \sqrt{\frac{\mu}{a^3}} \tag{16}$$

This formulation assumes a keplerian orbit and one can incorporate perturbations by adding secular variations such that the target's orbital elements varies with time which slightly improves the accuracy of the solution. The main perturbing affects lie within the relative orbital elements as will be shown in the following sections.

III. State Transition Matrix Formulation

This section presents the formulation used to create the state transiton matrix that maps the states at a time t_f to the initial states at t_0. To first formulate the state transition matrix the system dynamics must be defined by the derivative of the state vector, $\dot{\boldsymbol{x}}$, as a function of the states

$$\dot{\boldsymbol{x}} = \begin{bmatrix}\dot{a} & \dot{e} & \dot{i} & \dot{\omega} & \dot{\Omega} & \dot{M}\end{bmatrix}^T = \boldsymbol{f}(\boldsymbol{x}) \tag{17}$$

and the function is the combination of keplerian and total perturbing effects considered represented by

$$\boldsymbol{f}(\boldsymbol{x}) = \boldsymbol{f_{kep}}(\boldsymbol{x}) + \sum \boldsymbol{f_{perturb}}(\boldsymbol{x}) \tag{18}$$

where

$$\boldsymbol{f_{kep}}(\boldsymbol{x}) = \begin{bmatrix}0 & 0 & 0 & 0 & 0 & n\end{bmatrix}^T \tag{19}$$

$$\boldsymbol{f_{perturb}}(\boldsymbol{x}) = \begin{bmatrix}\dot{a}_{perturb} & \dot{e}_{perturb} & \dot{i}_{perturb} & \dot{\omega}_{perturb} & \dot{\Omega}_{perturb} & \dot{M}_{perturb}\end{bmatrix}^T \tag{20}$$

The system dynamics can now be expressed in terms of relative orbital elements by taking the Jacobian of eq. (17) as such

$$\Delta\dot{\boldsymbol{x}} = \boldsymbol{F}(\boldsymbol{x})\Delta\boldsymbol{x} \tag{21}$$

where

$$\boldsymbol{F}(\boldsymbol{x}) = \left.\frac{\partial \boldsymbol{F}(\boldsymbol{x})}{\partial \boldsymbol{x}}\right|_{\boldsymbol{x}=\boldsymbol{x}_t} \tag{22}$$

Now that the system dynamics have been defined, it can be linearized through a Taylor series expansion about the target's states such that

$$\Delta\boldsymbol{x}_f = \left[\boldsymbol{I}_{6\times 6} + \boldsymbol{F}(\boldsymbol{x})\Delta t + \frac{\boldsymbol{F}^2(\boldsymbol{x})}{2!}\Delta t^2 + \frac{\boldsymbol{F}^3(\boldsymbol{x})}{3!}\Delta t^3 ...\right]\Delta\boldsymbol{x}_0 \tag{23}$$

where $\Delta t = t_f - t_0$ and the Jacobian matrix $\boldsymbol{F}(\boldsymbol{x})$ is evaluated at the target's initial states. The Keplerian Jacobian is found as

*http://web.mit.edu/10.001/Web/Course_Notes/NLAE/node6.html

$$
\boldsymbol{F}_{kep}(\boldsymbol{x}) = \begin{bmatrix} 0 & 0 & 0 & 0 & 0 & 0 \\ 0 & 0 & 0 & 0 & 0 & 0 \\ 0 & 0 & 0 & 0 & 0 & 0 \\ 0 & 0 & 0 & 0 & 0 & 0 \\ 0 & 0 & 0 & 0 & 0 & 0 \\ -1.5n/a & 0 & 0 & 0 & 0 & 0 \end{bmatrix} \tag{24}
$$

Recently, Kuiack and Ulrich [22] developed a model which only includes the second zonal harmonic in terms of its secular and short periodic variations based off of Brouwer's [19] gravitational equations. Vinti [24] expanded on Brouwer's [19] and Kozai's [21] work to include the effects of the residual fourth zonal harmonic. In addition, an analytical relative dynamics for a J_2 perturbed elliptical orbit was formulated by Hamel and Lafontaine [25] but only included secular variations of RAAN, argument of perigee and mean anomaly. Liu [20] expanded on Brouwer's and Kozai's work to include secular variations of eccentricity and inclination, and concluded that their effects are small (about 0.5% more accurate). This paper uses the secular equations reformulated by Liu [20] and also given by Vallado [23] as a basis to derive the gravitational field Jacobian matrices $\boldsymbol{F_J}(\boldsymbol{x})$. The Jacobian matrix was derived, based on Liu's model [20], as

$$
\boldsymbol{F}_J(\boldsymbol{x}) = \begin{bmatrix} 0 & 0 & 0 & 0 & 0 & 0 \\ {F_J}^{21} & {F_J}^{22} & {F_J}^{23} & {F_J}^{24} & 0 & 0 \\ {F_J}^{31} & {F_J}^{32} & {F_J}^{33} & {F_J}^{34} & 0 & 0 \\ {F_J}^{41} & {F_J}^{42} & {F_J}^{43} & 0 & 0 & 0 \\ {F_J}^{51} & {F_J}^{52} & {F_J}^{53} & 0 & 0 & 0 \\ {F_J}^{61} & {F_J}^{62} & {F_J}^{63} & 0 & 0 & 0 \end{bmatrix} \tag{25}
$$

where

$$
\begin{aligned}
{F_J}^{21} &= \frac{1}{64a^8(e^2-1)^3 n}\left[3R_E^3\mu\sin(i)(144J_3 a\cos(\omega) - 180J_3 a\cos(\omega)\sin^2(i) - 144J_3 a e^2\cos(\omega))\right. \\
&+ +165J_2^2 R_E e\sin(2\omega)\sin^3(i) + 330J_4 R_E e\sin(2\omega)\sin(i) + 180J_3 a e^2\cos(\omega)\sin^2(i) \\
&+ \left. -154J_2^2 R_E e\sin(2\omega)\sin(i) - 385J_4 R_E e\sin(2\omega)\sin^3(i)\right]
\end{aligned} \tag{26}
$$

$$
\begin{aligned}
{F_J}^{22} &= -\frac{1}{32a^4(e^2-1)^3}\left[3J_2^2 R_E^4\sin(2\omega)\sin^2(i)n(15\sin^2(i)-14) + 15J_4 R_E^4\sin(2\omega)\sin^2(i)n(7\sin^2(i)-6)\right] \\
&+ \frac{1}{16a^4(e^2-1)^4}\left[9J_2^2 R_E^4 e^2\sin(2\omega)\sin^2(i)n(15\sin^2(i)-14) - 45J_4 R_E^4 e^2\sin(2\omega)\sin^2(i)n(7\sin^2(i)-6)\right] \\
&+ \frac{3J_3 R_E^3 e\cos(\omega)\sin(i)n(5\sin^2(i)-4)}{2a^3(e^2-1)^3}
\end{aligned} \tag{27}
$$

$$
\begin{aligned}
{F_J}^{23} &= -\frac{1}{(8a^4(e^2-1)^3)}\left[3R_E^3\cos(i)n(4J_3 a\cos(\omega) - 15J_3 a\cos(\omega)\sin^2(i) - 4J_3 a e^2\cos(\omega)\right. \\
&+ -15J_2^2 R_E e\sin(2\omega)\sin^3(i) + 15J_4 R_E e\sin(2\omega)\sin(i) + 15J_3 a e^2\cos(\omega)\sin^2(i) \\
&+ \left. +7J_2^2 R_E e\sin(2\omega)\sin(i) - 35J_4 R_E e\sin(2\omega)\sin^3(i))\right]
\end{aligned} \tag{28}
$$

$$
\begin{aligned}
{F_J}^{24} &= \frac{1}{16a^4(e^2-1)^3}\left[15J_4 R_E^4 e\cos(2\omega)\sin^2(i)n(7\sin^2(i)-6) - 3J_2^2 R_E^4 e\cos(2\omega)\sin^2(i)n(15\sin^2(i)-14)\right] \\
&+ \frac{3J_3 R_E^3\sin(i)\sin(\omega)n(5\sin^2(i)-4)}{8a^3(e^2-1)^2}
\end{aligned} \tag{29}
$$

$$
\begin{aligned}
{F_J}^{31} = & -\frac{3R_E^3 e\mu}{128a^8(e^2-1)^4 n}\left[360J_3 a\cos^3(i)\cos(\omega) - 72J_3 a\cos(i)\cos(\omega) + 154J_2^2 R_E e\sin(2i)\sin(2\omega)\right. \\
& + +72J_3 ae^2\cos(i)\cos(\omega) - 360J_3 ae^2\cos^3(i)\cos(\omega) + 330J_4 R_E e\sin(2i)\sin(2\omega) \\
& \left. + -330J_2^2 R_E e\sin(2\omega)\cos(i)\sin^3(i) - 770J_4 R_E e\sin(2\omega)\cos(i)\sin^3(i)\right]
\end{aligned} \tag{30}
$$

$$
\begin{aligned}
{F_J}^{32} = & \frac{3J_2^2 R_E^4 e^3\sin(2i)\sin(2\omega)n(15\sin^2(i)-14)}{8a^4(e^2-1)^5} + \frac{15J_4 R_E^4 e^3\sin(2i)\sin(2\omega)n(7\sin^2(i)-6)}{8a^4(e^2-1)^5} \\
& - \frac{15J_4 R_E^4 e\sin(2i)\sin(2\omega)n(7\sin^2(i)-6)}{32a^4(e^2-1)^4} - \frac{3J_2^2 R_E^4 e\sin(2i)\sin(2\omega)n(15\sin^2(i)-14)}{32a^4(e^2-1)^4} \\
& - \frac{3J_3 R_E^3\cos(i)\cos(\omega)n(5\cos^2(i)-1)}{8a^3(e^2-1)^3} + \frac{9J_3 R_E^3 e^2\cos(i)\cos(\omega)n(5\cos^2(i)-1)}{4a^3(e^2-1)^4}
\end{aligned} \tag{31}
$$

$$
\begin{aligned}
{F_J}^{33} = & \frac{1}{16a^4(e^2-1)^4}\left[3R_E^3 e\cos(\omega)n(30J_3 a\sin^3(i) - 28J_3 a\sin(i) - 30J_3 ae^2\sin^3(i) + 30J_4 R_E e\sin(\omega)\right. \\
& +14J_2^2 R_E e\sin(\omega) + 28J_3 ae^2\sin(i) - 165J_4 R_E e\sin^2(i)\sin(\omega) + 140J_4 R_E e\sin^4(i)\sin(\omega) \\
& \left. -73J_2^2 R_E e\sin^2(i)\sin(\omega) + 60J_2^2 R_E e\sin^4(i)\sin(\omega))\right]
\end{aligned} \tag{32}
$$

$$
\begin{aligned}
{F_J}^{34} = & \frac{3J_3 R_E^3 e\cos(i)\sin(\omega)n(5\cos^2(i)-1)}{8a^3(e^2-1)^3} - \frac{3J_2^2 R_E^4 e^2\cos(2\omega)\sin(2i)n(15\sin^2(i)-14)}{32a^4(e^2-1)^4} \\
& - \frac{15J_4 R_E^4 e^2\cos(2\omega)\sin(2i)n(7\sin^2(i)-6)}{32a^4(e^2-1)^4}
\end{aligned} \tag{33}
$$

$$
\begin{aligned}
{F_J}^{41} = & -\frac{3R_E^2\mu}{256a^8(e^2-1)^4 n}\left[3520J_4 R_E^2 + 896J_2 a^2 + 3960J_4 R_E^2 e^2 - 1792J_2 a^2 e^2 + 896J_2 a^2 e^4 + 616J_2^2 R_E^2 e^2\right. \\
& - 13640J_4 R_E^2\sin^2(i) + 10780J_4 R_E^2\sin^4(i) - 1120J_2 a^2\sin^2(i) + 8360J_2^2 R_E^2\sin^2(i) \\
& - 9790J_2^2 R_E^2\sin^4(i) - 13860J_4 R_E^2 e^2\sin^2(i) + 10395J_4 R_E^2 e^2\sin^4(i) + 2240J_2 a^2 e^2\sin^2(i) \\
& \left. - 1120J_2 a^2 e^4\sin^2(i) - 396J_2^2 R_E^2 e^2\sin^2(i) - 495J_2^2 R_E^2 e^2\sin^4(i)\right]
\end{aligned} \tag{34}
$$

$$
\begin{aligned}
{F_J}^{42} = & -\frac{3R_E^2 en}{64a^4(e^2-1)^5}\left[1640J_4 R_E^2 + 256J_2 a^2 + 56J_2^2 R_E^2 + 1080J_4 R_E^2 e^2 - 512J_2 a^2 e^2 + 256J_2 a^2 e^4\right. \\
& + 168J_2^2 R_E^2 e^2 - 6220J_4 R_E^2\sin^2(i) + 4865J_4 R_E^2\sin^4(i) - 320J_2 a^2\sin^2(i) + 3004J_2^2 R_E^2\sin^2(i) \\
& - 3605J_2^2 R_E^2\sin^4(i) - 3780J_4 R_E^2 e^2\sin^2(i) + 2835J_4 R_E^2 e^2\sin^4(i) + 640J_2 a^2 e^2\sin^2(i) \\
& \left. - 320J_2 a^2 e^4\sin^2(i) - 108J_2^2 R_E^2 e^2\sin^2(i) - 135J_2^2 R_E^2 e^2\sin^4(i)\right]
\end{aligned} \tag{35}
$$

$$
\begin{aligned}
{F_J}^{43} = & -15J_4 R_E^4 n\left[\frac{2\cos(i)\sin(i)(252e^2+248) - 4\cos(i)\sin^3(i)(189e^2+196)}{128a^4(e^2-1)^4}\right] \\
& - 3J_2^2 R_E^4 n\left[\frac{2\cos(i)\sin(i)(36e^2-760) + 4\cos(i)\sin^3(i)(45e^2+890)}{128a^4(e^2-1)^4}\right] \\
& - \frac{15J_2 R_E^2\cos(i)\sin(i)n}{2a^2(e^2-1)^2}
\end{aligned} \tag{36}
$$

$$
\begin{aligned}
{F_J}^{51} = & \frac{3R_E^2\mu\cos(i)}{64a^8(e^2-1)^4 n}\left[330J_4 R_E^2 + 112J_2 a^2 + 748J_2^2 R_E^2 + 495J_4 R_E^2 e^2 - 224J_2 a^2 e^2 + 112J_2 a^2 e^4\right. \\
& \left. + 99J_2^2 R_E^2 e^2 - 770J_4 R_E^2\cos^2(i) - 880J_2^2 R_E^2\cos^2(i)^2 - 1155J_4 R_E^2 e^2\cos^2(i) - 55J_2^2 R_E^2 e^2\cos^2(i)\right]
\end{aligned} \tag{37}
$$

$$
\begin{aligned}
{F_J}^{52} = & \frac{3R_E^2 e\cos(i)n}{16a^4(e^2-1)^5}\left[32J_2 a^2 - 220J_4 R_E^2 - 44J_2^2 R_E^2 - 180J_4 R_E^2 e^2 - 64J_2 a^2 e^2 + 32J_2 a^2 e^4\right. \\
& \left. + 12J_2^2 R_E^2 e^2 + 385J_4 R_E^2\sin^2(i) + 325J_2^2 R_E^2\sin^2(i) + 315J_4 R_E^2 e^2\sin^2(i) + 15J_2^2 R_E^2 e^2\sin^2(i)\right]
\end{aligned} \tag{38}
$$

$$
\begin{aligned}
F_J{}^{53} = &\frac{3R_E^2\sin(i)n}{32a^4(e^2-1)^4}\left[16J_2a^2 - 180J_4R_E^2 - 172J_2^2R_E^2 - 270J_4R_E^2e^2 - 32J_2a^2e^2 + 16J_2a^2e^4\right.\\
&\left.- 6J_2^2R_E^2e^2 + 210J_4R_E^2\sin^2(i) + 240J_2^2R_E^2\sin^2(i) + 315J_4R_E^2e^2\sin^2(i) + 15J_2^2R_E^2e^2\sin^2(i)\right]
\end{aligned}
\tag{39}
$$

$$
\begin{aligned}
F_J{}^{61} = &-\frac{1}{1024a^8(1-e^2)^{9/2}n}\left[52800J_2^2R_E^4\mu\sin^2(i) - 69168J_2^2R_E^4\mu\sin(i)^4 + 10560J_2^2R_E^4e^2\mu\right.\\
&+ -9240J_2^2R_E^4e^4\mu - 5376J_2R_E^2a^2\mu(e^2-1)^3 - 51744J_2^2R_E^4e^2\mu\sin^2(i) + 35376J_2^2R_E^4e^2\mu\sin(i)^4\\
&+ +10824J_2^2R_E^4e^4\mu\sin^2(i) + 2607J_2^2R_E^4e^4\mu\sin(i)^4 + 15840J_4R_E^4e^2\mu(e^2-1)\\
&+ +8064J_2R_E^2a^2\mu\sin^2(i)(e^2-1)^3 - 79200J_4R_E^4e^2\mu\sin(i)(e^2-1)\\
&\left.+ +69300J_4R_E^4e^2\mu\sin^2(i)(e^2-1)\right]
\end{aligned}
\tag{40}
$$

$$
\begin{aligned}
F_J{}^{62} = &\,3J_2^2R_E^4n\frac{640e - 1120e^3 + \sin^4(i)(316e^3 + 2144e) - \sin^2(i)(-1312e^3 + 3136e)}{512a^4(1-e^2)^{9/2}}\\
&- \frac{9J_2R_E^2en(3\sin^2(i)^2 - 2)}{4a^2(1-e^2)^{5/2}} - \frac{45J_4R_E^4en(35\sin^2(i) - 40\sin(i) + 8)}{64a^4(1-e^2)^{7/2}}\\
&+ 27J_2^2R_E^4en\left[\frac{\sin^4(i)(79e^4 + 1072e^2 - 2096) + \sin^2(i)(328e^4 - 1568e^2 + 1600) + 320e^2 - 280e^4}{512a^4(1-e^2)^{11/2}}\right]\\
&- \frac{315J_4R_E^4e^3n(35\sin^2(i) - 40\sin(i) + 8)}{128a^4(1-e^2)^{9/2}}
\end{aligned}
\tag{41}
$$

$$
\begin{aligned}
F_J{}^{63} = &\,3J_2^2R_E^4n\left[\frac{4\cos(i)\sin^3(i)(79e^4 + 1072e^2 - 2096) + 2\cos(i)\sin(i)(328e^4 - 1568e^2 + 1600)}{512a^4(1-e^2)^{9/2}}\right]\\
&+ 45J_4R_E^4e^2n\frac{40\cos(i) - 70\cos(i)\sin(i)}{128a^4(1-e^2)^{7/2}} - \frac{9J_2R_E^2\cos(i)\sin(i)n}{2a^2(1-e^2)^{3/2}}
\end{aligned}
\tag{42}
$$

where J_2, J_3 and J_4 are the second, third and fourth zonal harmonics respectively, R_E is the mean radius of the Earth, μ is the gravitational constant of Earth and n is the mean orbital motion of the satellite.

The effects of third body perturbations on satellite orbits has been studied extensively in the past and continues to be in the present. Kozai [17] developed the first secular and long-periodic equations on the effects of luni-solar perturbations on a satellite's orbital elements in 1959 based on the assumption that the distance of the satellite from the Earth was very small compared to the moon and that the moon's orbit is circular. Those equations were re-visited by him in 1973 to include short periodic terms [16]. Smith [26, 27] extended Kozai's theory to include secular changes for a third body in an elliptical orbit and found that for NASA's Echo 1 mission in 1960, the perigee radius decreased as much as 100 meters over 25 days. Luni-solar effects on orbital elements were also developed by Cook [28] in 1961 who also included the effects of solar radiation pressure, Kaula [29] in 1962 and Giacagla[30] in 1974 who also developed secular and periodic variations. Furthermore, Musen, et al. [31] expanded on Kozai's theory in 1961 where they observed that the third body perturbation causes the perigee height of a satellite to increase with periodic variations over long durations (20 km increase over approximately one month duration) due to third body effects on eccentricity. Recently, Domingos, et al. [15] and Prado [14], developed a simplified analytical model for a satellite's orbital elements based on the third body disturbing function expanded in Legendre polynomials up to fourth order. Specifically, the developed analytical model double averaged the expanded disturbing function over the satellite's orbital period and then again over the third body's. The third body Jacobian matrix derived in this work, based on Prado's double averaged model [14] expanded to the fourth order, is provided as

$$
\boldsymbol{F}_{3rd}(\boldsymbol{x}) = \begin{bmatrix}
0 & 0 & 0 & 0 & 0 & 0\\
F_{3rd}{}^{21} & F_{3rd}{}^{22} & F_{3rd}{}^{23} & F_{3rd}{}^{24} & 0 & 0\\
F_{3rd}{}^{31} & F_{3rd}{}^{32} & F_{3rd}{}^{33} & F_{3rd}{}^{34} & 0 & 0\\
F_{3rd}{}^{41} & F_{3rd}{}^{42} & F_{3rd}{}^{43} & F_{3rd}{}^{44} & 0 & 0\\
F_{3rd}{}^{51} & F_{3rd}{}^{52} & F_{3rd}{}^{53} & F_{3rd}{}^{54} & 0 & 0\\
F_{3rd}{}^{61} & F_{3rd}{}^{62} & F_{3rd}{}^{63} & F_{3rd}{}^{64} & 0 & 0
\end{bmatrix}
\tag{43}
$$

where

$$F_{3rd}{}^{21} = \frac{45e\mu K n'^{2}(1-e^2)^{1/2}}{16384a^4a'^2n}\Big[588a^2\sin(2\omega)+294a^2e^2\sin(2\omega)+3087a^2e^2\sin(4\omega)$$
$$+\ 784a^2\cos(2i)\sin(2\omega)+1024a'^{2}\sin(2\omega)\sin^2(i)+392a^2e^2\cos(2i)\sin(2\omega)-4116a^2e^2\cos(2i)\sin(4\omega)\Big] \tag{44}$$

$$F_{3rd}{}^{22} = -\frac{15Kn'^{2}}{8192(1-e^2)^{1/2}a'^2n}\Big[126a^2e^2\sin(2\omega)-252a^2\sin(2\omega)-3969a^2e^2\sin(4\omega)+504a^2e^4\sin(2\omega)$$
$$+5292a^2e^4\sin(4\omega)-336a^2\cos(2i)\sin(2\omega)-1024a'^{2}\sin(2\omega)\sin^2(i)+168a^2e^2\cos(2i)\sin(2\omega)$$
$$+5292a^2e^2\cos(2i)\sin(4\omega)+672a^2e^4\cos(2i)\sin(2\omega)-7056a^2e^4\cos(2i)\sin(4\omega)+2048a'^{2}e^2\sin(2\omega)\sin^2(i)\Big] \tag{45}$$

$$F_{3rd}{}^{23} = -\frac{15eKn'^{2}(1-e^2)^{1/2}}{1024a'^2n}\Big[84a^2\sin(2i)\sin(2\omega)-256a'^{2}\sin(2\omega)\cos(i)\sin(i)+42a^2e^2\sin(2i)\sin(2\omega)$$
$$-\ 441a^2e^2\sin(2i)\sin(4\omega)\Big] \tag{46}$$

$$F_{3rd}{}^{24} = \frac{15eKn'^{2}\cos(2\omega)\sin^2(i)(1-e^2)^{1/2}}{4n}+\frac{9a^2Kn'^{2}(1-e^2)^{1/2}}{65536a'^2n}\Big[2e^3\cos(2\omega)(4480\cos^2(i)-560)$$
$$-\ 4e^3(2\cos^2(2\omega)-1)(47040\cos^2(i)-41160)+2e\cos(2\omega)(8960\cos^2(i)-1120)\Big] \tag{47}$$

$$F_{3rd}{}^{31} = -\frac{45e^2Kn'^{2}\sin(2\omega)\cos(i)}{8192aa'^{2}\sin(i)(1-e^2)^{1/2}n}\Big[784a^2\cos^2(i)-512a'^{2}\cos^2(i)-98a^2+512a'^{2}-49a^2e^2$$
$$+\ 392a^2e^2\cos^2(i)+7203a^2e^2\cos(2\omega)-8232a^2e^2\cos(2\omega)\cos^2(i)\Big] \tag{48}$$

$$F_{3rd}{}^{32} = -\frac{15eKn'^{2}\sin(2\omega)\cos(i)}{4096a'^{2}\sin(i)(1-e^2)^(3/2)n}\Big[672a^2\cos^2(i)+1024a'^{2}\sin^2(i)-84a^2-42a^2e^2+63a^2e^4$$
$$+\ 336a^2e^2\cos^2(i)-504a^2e^4\cos^2(i)+12348a^2e^2\cos(2\omega)-9261a^2e^4\cos(2\omega)-512a'^{2}e^2\sin^2(i)$$
$$-\ 14112a^2e^2\cos(2\omega)\cos^2(i)+10584a^2e^4\cos(2\omega)\cos^2(i)\Big] \tag{49}$$

$$F_{3rd}{}^{33} = -\frac{15e^2Kn'^{2}\sin(2\omega)}{4096a'^2(1-e^2)^{1/2}(\cos^2(i)-1)n}\Big[1008a^2\cos^2(i)-672a^2\cos^4(i)-1536a'^{2}\cos^2(i)$$
$$+\ 1024a'^{2}\cos^4(i)-42a^2+512a'^{2}-21a^2e^2+504a^2e^2\cos^2(i)-336a^2e^2\cos^4(i)$$
$$+\ 3087a^2e^2\cos(2\omega)-10584a^2e^2\cos(2\omega)\cos^2(i)+7056a^2e^2\cos(2\omega)\cos^4(i)\Big] \tag{50}$$

$$F_{3rd}{}^{34} = -\frac{15e^2Kn'^{2}\cos(2\omega)\cos(i)\sin(i)}{4(1-e^2)^{1/2}n}-\frac{9a^2Kn'^{2}\cos(i)}{65536a'^{2}\sin(i)(1-e^2)^{1/2}n}\Big[2e^4\cos(2\omega)(4480\cos^2(i)-560)$$
$$+\ 2e^2\cos(2\omega)(8960\cos^2(i)-1120)-4e^4(2\cos(2\omega)^2-1)(47040\cos^2(i)-41160)\Big] \tag{51}$$

$$F_{3rd}{}^{41} = \frac{9\mu Kn'^{2}}{16384a^4a'^2(1-e^2)^{1/2}n^3}\Big[54880a^2\cos^4(i)-40320a^2\cos^2(i)+5120a'^{2}\cos^2(i)-980a^2\cos(2\omega)$$
$$+\ 5120a'^{2}\cos(2\omega)+3360a^2-1024a'^{2}-36855a^2e^2+33495a^2e^4+1024a'^{2}e^2+15960a^2e^2\cos^2(i)$$
$$+\ 68600a^2e^2\cos^4(i)+12600a^2e^4\cos^2(i)-41160a^2e^4\cos^4(i)+980a^2e^4\cos(2\omega)-5120a'^{2}e^2\cos(2\omega)$$
$$+\ 72030a^2e^2\cos(2\omega)^2-72030a^2e^4\cos(2\omega)^2+7840a^2\cos(2\omega)\cos^2(i)-5120a'^{2}\cos(2\omega)\cos^2(i)$$
$$+\ 62720a^2e^2\cos(2\omega)\cos^2(i)-109760a^2e^2\cos(2\omega)\cos^4(i)+23520a^2e^4\cos(2\omega)\cos^2(i)$$
$$-\ 54880a^2e^4\cos(2\omega)\cos^4(i)-82320a^2e^2\cos(2\omega)^2\cos^2(i)+82320a^2e^4\cos(2\omega)^2\cos^4(i)\Big] \tag{52}$$

$$
\begin{aligned}
F_{3rd}{}^{42} = & -\frac{3eKn'^{2}}{8192a'^{2}(1-e^{2})^{(}3/2)n}\Big[3600a^{2}\cos^{2}(i)-82320a^{2}\cos^{4}(i)-5120a'^{2}\cos^{2}(i)+420a^{2}\cos(2\omega)\\
&+5120a'^{2}\cos(2\omega)-61740a^{2}\cos(2\omega)^{2}+30150a^{2}-1024a'^{2}-73215a^{2}e^{2}+43065a^{2}e^{4}+1024a'^{2}e^{2}\\
&-14760a^{2}e^{2}\cos^{2}(i)+99960a^{2}e^{2}\cos^{4}(i)+16200a^{2}e^{4}\cos^{2}(i)-52920a^{2}e^{4}\cos^{4}(i)-1680a^{2}e^{2}\cos(2\omega)\\
&+1260a^{2}e^{4}\cos(2\omega)-5120a'^{2}e^{2}\cos(2\omega)+154350a^{2}e^{2}\cos(2\omega)^{2}-92610a^{2}e^{4}\cos(2\omega)^{2}\\
&-57120a^{2}\cos(2\omega)\cos^{2}(i)+94080a^{2}\cos(2\omega)\cos^{4}(i)+5120a'^{2}\cos(2\omega)\cos^{2}(i)\\
&+70560a^{2}\cos(2\omega)^{2}\cos^{2}(i)-13440a^{2}e^{2}\cos(2\omega)\cos^{2}(i)+47040a^{2}e^{2}\cos(2\omega)\cos^{4}(i)\\
&+30240a^{2}e^{4}\cos(2\omega)\cos^{2}(i)-70560a^{2}e^{4}\cos(2\omega)\cos^{4}(i)-35280a^{2}e^{2}\cos(2\omega)^{2}\cos^{2}(i)\\
&-141120a^{2}e^{2}\cos(2\omega)^{2}\cos^{4}(i)+105840a^{2}e^{4}\cos(2\omega)^{2}\cos^{4}(i)\Big]
\end{aligned}\tag{53}
$$

$$
\begin{aligned}
F_{3rd}{}^{43} = & \frac{15Kn'^{2}\cos(i)(\cos^{2}(i)-1)}{512a'^{2}\sin(i)(1-e^{2})^{1/2}n}\Big[1176a^{2}\cos^{2}(i)+84a^{2}\cos(2\omega)-128a'^{2}\cos(2\omega)-432a^{2}\\
&+128a'^{2}+171a^{2}e^{2}+135a^{2}e^{4}+1470a^{2}e^{2}\cos^{2}(i)-882a^{2}e^{4}\cos^{2}(i)+672a^{2}e^{2}\cos(2\omega)\\
&+252a^{2}e^{4}\cos(2\omega)-882a^{2}e^{2}\cos(2\omega)^{2}-2352a^{2}e^{2}\cos(2\omega)\cos^{2}(i)\\
&-1176a^{2}e^{4}\cos(2\omega)\cos^{2}(i)+1764a^{2}e^{4}\cos(2\omega)^{2}\cos^{2}(i)\Big]
\end{aligned}\tag{54}
$$

$$
\begin{aligned}
F_{3rd}{}^{44} = & \frac{3Kn'^{2}\sin(2\omega)(5\cos^{2}(i)+5e^{2}-5)}{4(1-e^{2})^{1/2}n}-\frac{9a^{2}Kn'^{2}(1-e^{2})^{1/2}}{32768a'^{2}n}\left[2\sin(2\omega)(2240\cos(2i)+1680)\right.\\
&\left.+2e^{2}\sin(2\omega)(2240\cos(2i)+1680)-4e^{2}\sin(4\omega)(11760\cos(2i)-8820)\right]\\
&-\frac{9a^{2}Kn'^{2}\cos(i)}{65536a'^{2}\sin(i)(1-e^{2})^{1/2}n}\left[2e^{4}\sin(2\omega)(2240\sin(2i)-7840\sin(4i))\right.\\
&\left.-4e^{4}\sin(4\omega)(11760\sin(2i)-5880\sin(4i))+2e^{2}\sin(2\omega)\left[4480\sin(2i)-15680\sin(4i)\right]\right]
\end{aligned}\tag{55}
$$

$$
\begin{aligned}
F_{3rd}{}^{51} = & \frac{1}{16384aa'^{2}\mu\sin(i)(1-e^{2})^{1/2}n}\Big[5040a^{2}\mu Kn'^{2}\sin(2i)(e^{2}-1)-9216a'^{2}\mu Kn'^{2}\sin(2i)\\
&+17640a^{2}\mu Kn'^{2}\sin(4i)(e^{2}-1)-13824a'^{2}e^{2}\mu Kn'^{2}\sin(2i)+25200a^{2}e^{2}\mu Kn'^{2}\sin(2i)(e^{2}-1)\\
&+88200a^{2}e^{2}\mu Kn'^{2}\sin(4i)(e^{2}-1)+9450a^{2}e^{4}\mu Kn'^{2}\sin(2i)(e^{2}-1)\\
&+33075a^{2}e^{4}\mu Kn'^{2}\sin(4i)(e^{2}-1)+35280a^{2}e^{2}\mu Kn'^{2}\cos(2\omega)\sin(2i)(e^{2}-1)\\
&-123480a^{2}e^{2}\mu Kn'^{2}\cos(2\omega)\sin(4i)(e^{2}-1)+17640a^{2}e^{4}\mu Kn'^{2}\cos(2\omega)\sin(2i)(e^{2}-1)\\
&-61740a^{2}e^{4}\mu Kn'^{2}\cos(2\omega)\sin(4i)(e^{2}-1)-92610a^{2}e^{4}\mu Kn'^{2}\cos(4\omega)\sin(2i)(e^{2}-1)\\
&+46305a^{2}e^{4}\mu Kn'^{2}\cos(4\omega)\sin(4i)(e^{2}-1)+46080a'^{2}e^{2}\mu Kn'^{2}\cos(2\omega)\cos(i)\sin(i)\Big]
\end{aligned}\tag{56}
$$

$$
\begin{aligned}
F_{3rd}{}^{52} = & \frac{3eKn'^{2}\cos(i)(5\cos(2\omega)-3)}{4(1-e^{2})^{1/2}n}-\frac{3eKn'^{2}\cos(i)(3e^{2}-5e^{2}\cos(2\omega)+2)}{8(1-e^{2})^{(}3/2)n}\\
&-\frac{9a^{2}Kn'^{2}(1-e^{2})^{1/2}}{65536a'^{2}\sin(i)n}\Big[3200e(2\sin(2i)+7\sin(4i))+4e^{3}(1200\sin(2i)+4200\sin(4i))\\
&+2e\cos(2\omega)(4480\sin(2i)-15680\sin(4i))+4e^{3}\cos(2\omega)(2240\sin(2i)-7840\sin(4i))\\
&-4e^{3}\cos(4\omega)(11760\sin(2i)-5880\sin(4i))\Big]+\frac{9a^{2}eKn'^{2}}{65536a'^{2}\sin(i)(1-e^{2})^{1/2}n}\left[640\sin(2i)\right.\\
&+2240\sin(4i)+e^{4}(1200\sin(2i)+4200\sin(4i))+e^{2}(3200\sin(2i)+11200\sin(4i))\\
&+e^{4}\cos(2\omega)(2240\sin(2i)-7840\sin(4i))-e^{4}\cos(4\omega)(11760\sin(2i)-5880\sin(4i))\\
&\left.+e^{2}\cos(2\omega)(4480\sin(2i)-15680\sin(4i))\right]
\end{aligned}\tag{57}
$$

$$
\begin{aligned}
F_{3rd}{}^{53} = {} & \frac{3Kn'^2\sin(i)(3e^2-5e^2\cos(2\omega)+2)}{8(1-e^2)^{1/2}n} - \frac{9a^2Kn'^2(1-e^2)^{1/2}}{65536a'^2\sin(i)n}\,[1280\cos(2i)+8960\cos(4i) \\
& +e^4(2400\cos(2i)+16800\cos(4i))+e^2(6400\cos(2i)+44800\cos(4i)) \\
& +e^4\cos(2\omega)(4480\cos(2i)-31360\cos(4i))-e^4\cos(4\omega)(23520\cos(2i)-23520\cos(4i)) \\
& +e^2\cos(2\omega)(8960\cos(2i)-62720\cos(4i))\big] + \frac{9a^2Kn'^2\cos(i)(1-e^2)^{1/2}}{(65536a'^2\sin^2(i)n)}\,[640\sin(2i) \\
& +2240\sin(4i)+e^4(1200\sin(2i)+4200\sin(4i))+e^2(3200\sin(2i)+11200\sin(4i)) \\
& +e^4\cos(2\omega)(2240\sin(2i)-7840\sin(4i))-e^4\cos(4\omega)(11760\sin(2i)-5880\sin(4i)) \\
& +e^2\cos(2\omega)(4480\sin(2i)-15680\sin(4i))\big]
\end{aligned} \tag{58}
$$

$$
\begin{aligned}
F_{3rd}{}^{54} = {} & \frac{9a^2Kn'^2(1-e^2)^{1/2}}{65536a'^2\sin(i)n}\,\big[2e^4\sin(2\omega)(2240\sin(2i)-7840\sin(4i)) \\
& -4e^4\sin(4\omega)(11760\sin(2i)-5880\sin(4i))+2e^2\sin(2\omega)(4480\sin(2i)-15680\sin(4i))\big] \\
& -\frac{15e^2Kn'^2\sin(2\omega)\cos(i)}{4(1-e^2)^{1/2}n}
\end{aligned} \tag{59}
$$

$$
\begin{aligned}
F_{3rd}{}^{61} = {} & -\frac{3\mu Kn'^2}{16384a^4a'^2n^3}\,\big[211680a^2\sin^4(i)-265440a^2\sin^2(i)-6144a'^2\sin^2(i)-41160a^2\sin^2(\omega) \\
& +68964a^2+14336a'^2+167685a^2e^2+25305a^2e^4+6144a'^2e^2-474600a^2e^2\sin^2(i) \\
& +441000a^2e^2\sin^4(i)-840a^2e^4\sin^2(i)+88200a^2e^4\sin^4(i)+6144a'^2e^2\sin^2(i) \\
& -41160a^2e^2\sin^2(\omega)-123480a^2e^2\sin^4(\omega)+82320a^2e^4\sin^2(\omega)-123480a^2e^4\sin^4(\omega) \\
& +47040a^2\sin^2(i)\sin^2(\omega)-15360a'^2\sin^2(i)\sin^2(\omega)-799680a^2e^2\sin^2(i)\sin^2(\omega) \\
& +987840a^2e^2\sin^2(i)\sin^4(\omega)-940800a^2e^4\sin^2(i)\sin^2(\omega)+987840a^2e^4\sin^2(i)\sin^4(\omega) \\
& -15360a'^2e^2\sin^2(i)\sin^2(\omega)\big]
\end{aligned} \tag{60}
$$

$$
\begin{aligned}
F_{3rd}{}^{62} = {} & -\frac{3eKn'^2}{4096a'^2n}\,\big[63000a^2\sin^4(i)-67800a^2\sin^2(i)+2048a'^2\sin^2(i)-5880a^2\sin^2(\omega) \\
& -17640a^2\sin^4(\omega)+23955a^2+2048a'^2+7230a^2e^2-240a^2e^2\sin^2(i)+25200a^2e^2\sin^4(i) \\
& +23520a^2e^2\sin^2(\omega)-35280a^2e^2\sin^4(\omega)-114240a^2\sin^2(i)\sin^2(\omega)+141120a^2\sin^2(i)\sin^4(\omega) \\
& -5120a'^2\sin^2(i)\sin^2(\omega)-268800a^2e^2\sin^2(i)\sin^2(\omega)+282240a^2e^2\sin^2(i)\sin^4(\omega)\big]
\end{aligned} \tag{61}
$$

$$
\begin{aligned}
F_{3rd}{}^{63} = {} & \frac{3Kn'^2}{2048a'^2n}\,\big[1080a^2\sin(2i)+3780a^2\sin(4i)+1792a'^2\sin(2i)+2250a^2e^2\sin(2i) \\
& +7875a^2e^2\sin(4i)+450a^2e^4\sin(2i)+1575a^2e^4\sin(4i)+768a'^2e^2\sin(2i)+840a^2\cos(2\omega)\sin(2i) \\
& -2560a'^2\cos(i)\cos(\omega)^2\sin(i)+3360a^2e^2\cos(2\omega)\sin(2i)-4410a^2e^2\cos(4\omega)\sin(2i) \\
& +840a^2e^4\cos(2\omega)\sin(2i)-4410a^2e^4\cos(4\omega)\sin(2i)-2560a'^2e^2\cos(i)\cos(\omega)^2\sin(i)\big]
\end{aligned} \tag{62}
$$

$$
\begin{aligned}
F_{3rd}{}^{64} = {} & \frac{9a^2Kn'^2}{8192a'^2n}\,\big[2e^4\sin(2\omega)(1120\cos(2i)+840)+2e^2\sin(2\omega)(2240\cos(2i)+1680) \\
& -4e^4\sin(4\omega)(5880\cos(2i)-4410)\big]+\frac{Kn'^2\cos(\omega)\sin^2(i)\sin(\omega)(15e^2+15)}{4n} \\
& -\frac{9a^2Kn'^2(e^2-1)}{32768a'^2n}\,\big[2\sin(2\omega)(2240\cos(2i)+1680)+2e^2\sin(2\omega)(2240\cos(2i)+1680) \\
& -4e^2\sin(4\omega)(11760\cos(2i)-8820)\big]
\end{aligned} \tag{63}
$$

where $K = m'/(m' + m_0)$, m' is the mass of the third body, m_0 is the mass of the central body, n' is the mean orbital motion of the third body and a' is semi-major axis of the third body.

Although atmospheric drag is extensively studied, an exact or accurate model is yet to exist. One of the main reasons is the fact that density is difficult to model mainly due to the effects of solar wind activity on the atmosphere. However, analytical approximations of the effects of drag on orbital elements exist in literature based on the exponential model for density. The first analytical model was formulated by Izsak[32] in 1960 where he separated the effects in terms of periodic and secular variations. Xu, et al. [33] and Watson, et al. [34] also developed an analytical solution for drag, while Danielson[35] developed a semi-analytic solution and Martinusi, et al.[36] developed a first order accurate analytical solution. This paper focuses on the work of Blitzer [18] where he developed secular solutions for drag based on the exponential atmospheric model. This work derives the drag Jacobian matrix as

$$\boldsymbol{F}_{Drag}(\boldsymbol{x}) = \begin{bmatrix} {F_{Drag}}^{11} & {F_{Drag}}^{12} & {F_{Drag}}^{13} & 0 & 0 & 0 \\ {F_{Drag}}^{21} & {F_{Drag}}^{22} & {F_{Drag}}^{23} & 0 & 0 & 0 \\ {F_{Drag}}^{31} & {F_{Drag}}^{32} & {F_{Drag}}^{33} & {F_{Drag}}^{34} & 0 & 0 \\ {F_{Drag}}^{41} & {F_{Drag}}^{42} & {F_{Drag}}^{43} & {F_{Drag}}^{44} & 0 & 0 \\ {F_{Drag}}^{51} & {F_{Drag}}^{52} & {F_{Drag}}^{53} & {F_{Drag}}^{54} & 0 & 0 \\ 0 & 0 & 0 & 0 & 0 & 0 \end{bmatrix} \tag{64}$$

where

$$\begin{aligned} {F_{Drag}}^{11} =& -\frac{1}{8Hm(e+1)^{1/2}}\Big[C_D A a\rho exp(-c)(Hn(e+1)^{1/2} - 2aen(e+1)^{1/2} - 8H\omega_E\cos(i)(1-e)^{3/2} \\ &+4ae\omega_E\cos(i)(1-e)^{3/2})(4B_0 + 8B_1e + 3B_0e^2 + 3B_1e^3 + 3B_2e^2 + B_3e^3)\Big] \end{aligned} \tag{65}$$

$$\begin{aligned} {F_{Drag}}^{12} =& \frac{1}{Hm(e+1)^{1/2}}\Big[C_D A a^3\rho exp(-c)(n(e+1)^{1/2} - 2\omega_E\cos(i)(1-e)^{3/2})\times \\ &(B_0 + 2B_1e + 0.75B_0e^2 + 0.75B_1e^3 + 0.75B_2e^2 + 0.25B_3e^3)\Big] \\ &-\frac{1}{m(e+1)^{1/2}}\Big[C_D A a^2\rho exp(-c)(n(e+1)^{1/2} - 2\omega_E\cos(i)(1-e)^{3/2})\times \\ &(2B_1 + 1.5B_0e + 1.5B_2e + 2.5B_1e^2 + 0.75B_3e^2\Big] - \frac{1}{m(e+1)^{3/2}}\Big[2C_D A a^2\rho\omega_E exp(-c)\times \\ &\cos(i)(1-e)^{1/2}(e+2)(B_0 + 2B_1e + 0.75B_0e^2 + 0.75B_1e^3 + 0.75B_2e^2 + 0.25B_3e^3)\Big] \end{aligned} \tag{66}$$

$${F_{Drag}}^{13} = -\frac{2C_D A a^2\rho\omega_E exp(-c)\sin(i)(1-e)^{3/2}}{m(e+1)^{1/2}}\left[(B_0 + 2B_1e + (3e^2(B_0+B_2))/4 + (e^3(3B_1+B_3))/4)\right] \tag{67}$$

$$\begin{aligned} {F_{Drag}}^{21} =& \frac{C_D A\rho exp(-c)(Hn(e+1)^{1/2} + 2aen(e+1)^{1/2} + 4H\omega_E\cos(i)(1-e)^{3/2} - 4ae\omega_E\cos(i)(1-e)^{3/2})}{32Hm(e+1)^{1/2}} \\ &\times[(16B_1 + 8B_0e + 8B_2e - 5B_0e^3 - 10B_1e^2 - 4B_2e^3 - 2B_3e^2 + B_4e^3)] \end{aligned} \tag{68}$$

$$\begin{aligned} {F_{Drag}}^{22} =& \frac{C_D A a\rho exp(-c)(n(e+1)^{1/2} - 2\omega_E\cos(i)(1-e)^{3/2})}{m(e+1)^{1/2}}[1.25B_1e - 0.5B_2 - 0.5B_0 + 0.25B_3e \\ &+\frac{15}{16}B_0e^2 + 0.75B_2e^2 - \frac{3}{16}3B_4e^2\Big] + \frac{C_D A a^2\rho exp(-c)(n(e+1)^{1/2} - 2\omega_E\cos(i)(1-e)^{3/2})}{Hm(e+1)^{1/2}} \\ &\times\left[B_1 + 0.5B_0e + 0.5B_2e - \frac{3}{16}B_0e^3 - \frac{5}{8}B_1e^2 - 0.25B_2e^3 - 0.125B_3e^2 + \frac{1}{16}B_4e^3\right] \\ &-\frac{2C_D A a\rho\omega_E exp(-c)\cos(i)(1-e)^{1/2}(e+2)}{m(e+1)^{3/2}}\Bigg[B_1 + 0.5B_0e + 0.5B_2e - \frac{5}{16}B_0e^3 - \frac{5}{8}5B_1e^2 \\ &-0.25B_2e^3 - 0,125B_3e^2 + \frac{1}{16}B_4e^3\Bigg] \end{aligned} \tag{69}$$

$$
\begin{aligned}
{F_{Drag}}^{23} &= -\frac{2C_D A a\rho\omega_E exp(-c)\sin(i)(1-e)^{3/2}}{m(e+1)^{1/2}}\left[B_1 - 0.125e^2(5B_1+B_3)\right.\\
&\left.-\frac{1}{16}e^3(5B_0+4B_2-B_4)+0.5e(B_0+B_2)\right]
\end{aligned} \tag{70}
$$

$$
\begin{aligned}
{F_{Drag}}^{31} &= \frac{C_D A\rho\omega_E exp(-c)}{16Ha^3mn^3\left[1-(2\omega_E\cos(i)(1-e)^{3/2})/(n(e+1)^{1/2}))^{1/2}\right](e+1)^{1/2}}\times\\
&\left[7H\mu\omega_E\sin(2i)(1-e)^{3/2} - 4Ha^3\sin(i)n^3(e+1)^{1/2} + 4a^4e\sin(i)n^3(e+1)^{1/2}\right.\\
&\left.-4ae\mu\omega_E\sin(2i)(1-e)^{3/2}\right][B_0 - 2B_1e + B_2\cos(2\omega) - 2B_1e\cos(2\omega)]
\end{aligned} \tag{71}
$$

$$
\begin{aligned}
{F_{Drag}}^{32} &= \frac{C_D A a\rho\omega_E exp(-c)\sin(i)}{4m}\left[1-(2\omega_E\cos(i)(1-e)^{3/2})/(n(e+1)^{1/2})^{1/2}\right]\times\\
&[2B_1+2B_1\cos(2\omega)] + \frac{C_D A a^2\rho\omega_E exp(-c)\sin(i)}{4Hm}\left[1-(2\omega_E\cos(i)(1-e)^{3/2})/(n(e+1)^{1/2})^{1/2}\right]\\
&\times[B_0-2B_1e+\cos(2\omega)(B_2-2B_1e)] - \frac{C_D A a\rho\omega_E exp(-c)\sin(i)}{8m\left[1-(2\omega_E\cos(i)(1-e)^{3/2})/(n(e+1)^{1/2})^{1/2}\right]}\times\\
&\left[(3\omega_E\cos(i)(1-e)^{1/2})/(n(e+1)^{1/2}) + (\omega_E\cos(i)(1-e)^{3/2})/(n(e+1)^{3/2})\right]\times\\
&[B_0-2B_1e+\cos(2\omega)(B_2-2B_1e)]
\end{aligned} \tag{72}
$$

$$
\begin{aligned}
{F_{Drag}}^{33} &= -\frac{C_D A a\rho\omega_E exp(-c)}{4mnQ^{0.5}(e+1)^{1/2}}\left[\cos(i)n(e+1)^{1/2} - 2\omega_E\cos^2(i)(1-e)^{3/2} + \omega_E\sin^2(i)(1-e)^{3/2}\right]\\
&\times[B_0-2B_1e+B_2\cos(2\omega)-2B_1e\cos(2\omega)]
\end{aligned} \tag{73}
$$

$$
{F_{Drag}}^{34} = \left[C_D A a\rho\omega_E\sin(2\omega)exp(-c)sin(i)Q^{0.5}(B_2-2B_1e)\right]/(2m) \tag{74}
$$

$$
\begin{aligned}
{F_{Drag}}^{41} &= \frac{C_D A\rho\omega_E\sin(2\omega)exp(-c)\cos(i)(B_2-2B_1e)}{8Ha^3mn^3\left[1-(2\omega_E\cos(i)(e+1)^{3/2})/(n(e+1)^{1/2})\right]^{1/2}(e+1)^{1/2}}\times\\
&\left(2Ha^3n^3(e+1)^{1/2} - 2a^4en^3(e+1)^{1/2} - 7H\mu\omega_E\cos(i)(e+1)^{3/2} + 4ae\mu\omega_E\cos(i)(e+1)^{3/2}\right)
\end{aligned} \tag{75}
$$

$$
\begin{aligned}
{F_{Drag}}^{42} &= \frac{C_D A a\rho\omega_E\sin(2\omega)exp(-c)\cos(i)(B_2-2B_1e)}{8mQ^{0.5}}\left((3\omega_E\cos(i)(1-e)^{1/2})/(n(e+1)^{1/2})\right.\\
&\left.+(\omega_E\cos(i)(1-e)^{3/2})/(n(e+1)^{3/2})\right) - \left[B_1C_D A a\rho\omega_E\sin(2\omega)exp(-c)\cos(i)Q^{0.5}\right]/(2m)\\
&- C_D A a^2\rho\omega_E\sin(2\omega)exp(-c)\left[\cos(i)Q^{0.5}(B_2-2B_1e)\right]/(4Hm)
\end{aligned} \tag{76}
$$

$$
{F_{Drag}}^{43} = -\frac{C_D A a\rho\omega_E\sin(2\omega)exp(-c)\sin(i)(B_2-2B_1e)}{4mnQ^{0.5}(e+1)^{1/2}}\left[n(e+1)^{1/2} - 3\omega_E\cos(i)(1-e)^{3/2}\right] \tag{77}
$$

$$
{F_{Drag}}^{44} = C_D A a\rho\omega_E\cos(2\omega)exp(-c)\cos(i)Q^{0.5}(B_2-2B_1e)/(2m) \tag{78}
$$

$$
\begin{aligned}
{F_{Drag}}^{51} &= -\frac{C_D A\rho\omega_E\sin(2\omega)exp(-c)(B_2-2B_1e)}{8Ha^3mn^3Q^{0.5}(e+1)^{1/2}}\left[2Ha^3n^3(e+1)^{1/2} - 2a^4en^3(e+1)^{1/2}\right.\\
&\left.-7H\mu\omega_E\cos(i)(1-e)^{3/2} + 4ae\mu\omega_E\cos(i)(1-e)^{3/2}\right]
\end{aligned} \tag{79}
$$

$$
\begin{aligned}
{F_{Drag}}^{52} &= \frac{B_1C_D A a\rho\omega_E\sin(2\omega)exp(-c)Q^{0.5}}{2m} + \frac{C_D A a^2\rho\omega_E\sin(2\omega)exp(-c)Q^{0.5}(B_2-2B_1e)}{4Hm}\\
&- \frac{C_D A a\rho\omega_E\sin(2\omega)exp(-c)(B2-2B1e)}{8mQ^{1/2}}\left[\frac{3\omega_E\cos(i)(1-e)^{1/2}}{n(e+1)^{1/2}} + \frac{\omega_E\cos(i)(1-e)^{3/2}}{n(e+1)^{3/2}}\right]
\end{aligned} \tag{80}
$$

$$
{F_{Drag}}^{53} = -\frac{C_D A a\rho\omega_E^2\sin(2\omega)exp(-c)}{\left[4mnQ^{0.5}(e+1)^{1/2}\right]}\sin(i)(B_2-2B_1e)(1-e)^{3/2} \tag{81}
$$

$$
{F_{Drag}}^{54} = -C_D A a\rho\omega_E\cos(2\omega)exp(-c)Q^{1/2}(B_2-2B_1e)/(2m) \tag{82}
$$

where n, e, a, and ω are the mean orbital motion, eccentricity, semi-major axis and argument of perigee of a spacecraft respectively and ω_E is angular velocity of Earth. The density at the perigee ρ, modified Bessel function of the first kind B_j with argument c and the constants c and Q are given by

$$\rho = \rho_0 \exp(-\frac{h_p - h_0}{H}) \tag{83}$$

$$h_p = a(1-e) - R_E \tag{84}$$

$$B_j(c) = (\frac{c}{2})^j \sum_{k=0}^{\infty} \frac{(\frac{c}{2})^{2k}}{k!\Gamma(j+k+1)} \tag{85}$$

$$c = \frac{ae}{H} \tag{86}$$

$$Q = 1 - \frac{2\omega_E(1-e)^{1.5}}{n\sqrt{1+e}} \cos(i) \tag{87}$$

where ρ_0 is the atmospheric density in kg/m^3 and H is the scale height at a reference altitude h_0, h_p is altitude of perigee, Q is the factor for rotation of Earth's atmosphere (between 0.9-1.1), A is exposed area in m^2 to the direction of fluid flow and C_D is the coefficient of drag ranging from 1.5 to 3.0 for most spacecraft and m is mass of the spacecraft in kg. It should be noted when using these equations for drag, ρ must be multiplied by a factor of 1000 since the units for distance and speed are in km and km/s for spacecraft applications.

IV. Back-propagation guidance law

This section presents the procedure, summarized in steps, of the back-propagation guidance law by using the equations presented in the previous sections

1) A set of Keplerian osculating orbital elements are first initialized for the target: $[a_{t_0}, e_{t_0}, i_{t_0}, \omega_{t_0}, \Omega_{t_0}, \theta_{t_0}]^T$. Then, converting them to mean elements as described in Chihabi and Ulrich[37] such that the Jacobian matrices are evaluated as:

$$\boldsymbol{F}(\boldsymbol{x}) = \boldsymbol{F_{kep}}(\boldsymbol{x}) + \boldsymbol{F_J}(\boldsymbol{x}) + \boldsymbol{F_{3rd}}(\boldsymbol{x}) + \boldsymbol{F_{Drag}}(\boldsymbol{x}) \tag{88}$$

2) Select the desired LVLH coordinates, ie: $\boldsymbol{\rho}_f$ and $\dot{\boldsymbol{\rho}}_f$, and the desired time, Δt, the chaser is to drift into the desired coordinates.
3) The desired relative orbital elements, $\Delta \boldsymbol{x}_f$ can be found using Equations (3)-(16) and the following equation

$$\Delta \boldsymbol{x}_f = \begin{bmatrix} \boldsymbol{A}_{11} & \boldsymbol{A}_{12} \\ \boldsymbol{A}_{21} & \boldsymbol{A}_{22} \end{bmatrix}^{-1} \begin{bmatrix} \boldsymbol{\rho}_f \\ \dot{\boldsymbol{\rho}}_f \end{bmatrix} \tag{89}$$

4) Using Equation (23), the initial relative orbital elements are found as:

$$\Delta \boldsymbol{x}_0 = [\boldsymbol{I}_{6\times6} + \boldsymbol{F}(\boldsymbol{x})\Delta t]^{-1} \Delta \boldsymbol{x}_f \tag{90}$$

V. Numerical Simulations

This section presents a comparison of results obtained using the equations above against a numerical propagator that integrates the exact nonlinear differential equations of motion in $\mathcal{F}_I$ to verify the accuracy of the model. The numerical propagator integrates the inertial two-body equation of motion to which the inertial perturbing accelerations due to gravitational field by expanding the gravitational potential function up to degree and order 180, third body effects of the sun, moon and solar system planets, ocean and solid Earth tidal effects, relativity, solar radiation pressure, and drag were added then converted from $\mathcal{F}_I$ to $\mathcal{F}_L$.

The STM, proposed in this paper, was applied to the future Proba-3 mission and a chaser spacecraft in formation around Alouette-2 and was compared against the numerical propagator. Specifically, the results were compared with the results if the previous method presented in Chihabi and Ulrich [37]. Additionally, the back-propagation method presented in this paper was applied to Alouette-2 for rendezvous formation, for which a sensitivity analysis by varying the drift time was performed. The osculating orbital elements for the Proba-3 target spacecraft are initialized as a = 36944 km, e = 0.811, i = 59.0°, ω = 188°, Ω = 84.0°, and θ = 0° whereas for Alouette-2 they were initialized as a = 7947 km, e = 0.134, i = 79.8°, ω = 151.9°, Ω = 348.3°, and θ = 0°.

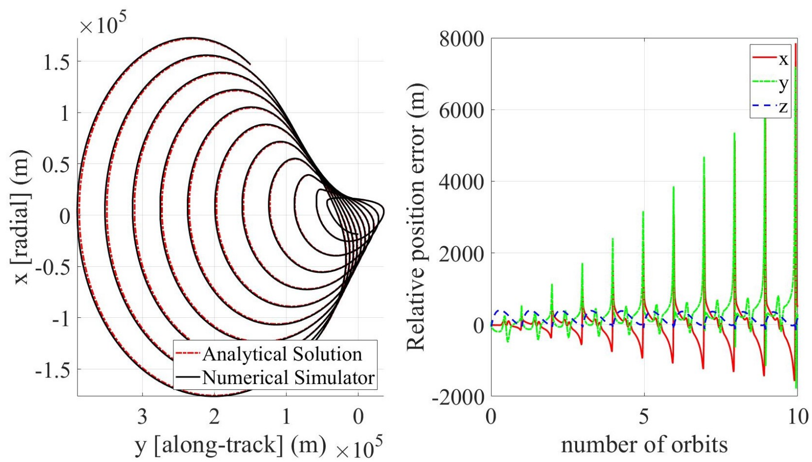

Fig. 1 Proba-3: Previous Solution

Figure 1 to Figure 3 show the results for the Proba-3 case, where the initial relative orbital elements were initialized as $\Delta\boldsymbol{x} = [0, 0.0005, 0, 0, 0, 0]^T$. Figure 1 shows the results for Proba-3 using the previous method outlined by Chihabi and Ulrich[37]. While Figure 2 and 3 show the results using the new STM formulation. Specifically, the former shows the results when incorporating secular variations of the target's orbital elements due to the gravitational field up to the fifth harmonic, third body perturbations due to the sun and moon, and drag into the $\boldsymbol{A}$ matrices that map the relative orbital elements to Cartesian coordinates while the latter assumes the matrices to be Keplerian. Using the STM with the target's varying orbital elements, the errors slightly increased by approximately 200 meters after 10 orbital periods for a separation distance of approximately 400 km in the along-track direction, excluding the effects of perturbations in the $\boldsymbol{A}$ matrices computations yield an increase in maximum error by approximately 7000 meters.

Figure 4 to Figure 6 show the results for the Alouette-2 case initialized with the same relative orbital elements as the Proba-3 case. When comparing Figures 4 and 5, the maximum error increased from near 5 meters to near 80 meters for a maximum separation distance of 7500 meters in the along-track direction while Figure 6 showed an increase to near 300 meters. While assuming the $\boldsymbol{A}$ matrices to be Keplerian yielded a significant increase in error when compared to the previous solution for the Proba-3 case, it is relatively insignificant when taking into the separation distance involved.

The proposed back propagation guidance law was validated against the same numerical simulator where the sensitivity to time was analyzed by varying the total time from $t_f = 2T$ to $t_f = 15T$ and plotted as shown in Figure 7 to Figure 12. In all cases, Alouette-2 was used as the target spacecraft and final desired cartesian coordinates were selected as 2 km in the along-track and radial directions, and 0 km in the in-track direction. In all cases the chaser drifted into the dired position with minimal error when compared to the numerical simulator. However, the main discrepancies were found with the desired time, where the desired along track position error increased as the desired time increased. For example, Figure 12 shows a desired time of 15 orbital periods having desired position errors were about 400 meters in the along-track direction and nearly meters 0 in the radial and in-track directions. On the other hand, Figure 10 shows a desired time of 8 orbital periods having desired position errors were less than 100 meters in the along-track direction and nearly 0 meters in the radial and in-track directions.

VI. Conclusion

Overall, this paper presented a simple, yet effective, method for both forward and back propagation guidance laws. Specifically, this paper integrates previously published results such that a new analytical solution that accurately predicts spacecraft relative motion was developed. When the analytical solution was compared to the numerical simulator, the relative motion yielded relatively small errors. The use of the STM allows for the guidance system to propagate relative motion as a LTI system, since the Jacobian matrices need only be calculated once. In other words, the new solution allows to propagate the relative orbital elements by the multiplication of constant matrices with time and initial relative orbital elements. Whereas the previous solution, presented in Chihabi and Ulrich [37], involved calculating new orbital elements at every time-step for both the target and the chaser spacecraft which are then used in Gurfil

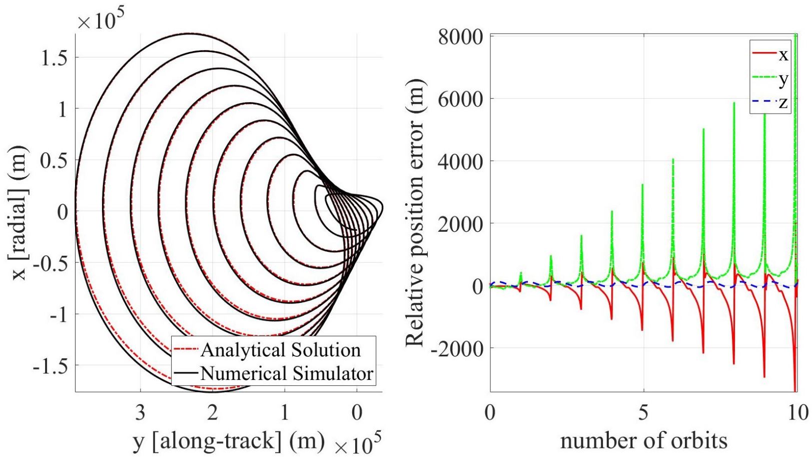

Fig. 2 Proba-3: STM, Varying Target Orbital Elements

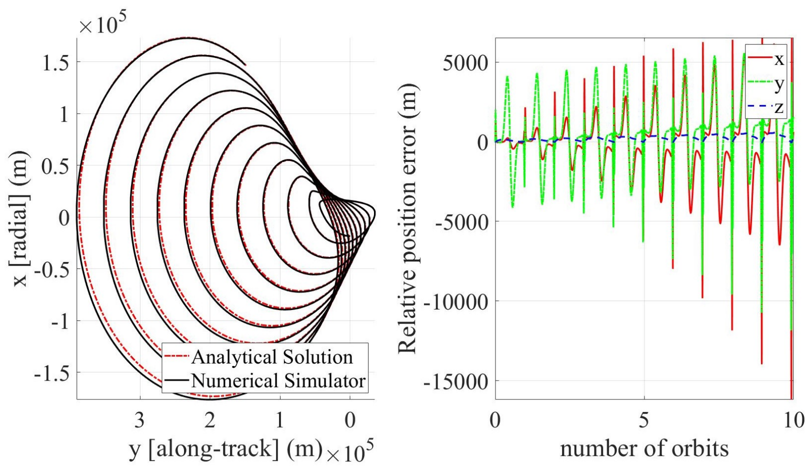

Fig. 3 Proba-3: STM, Invariant Target Orbital Elements

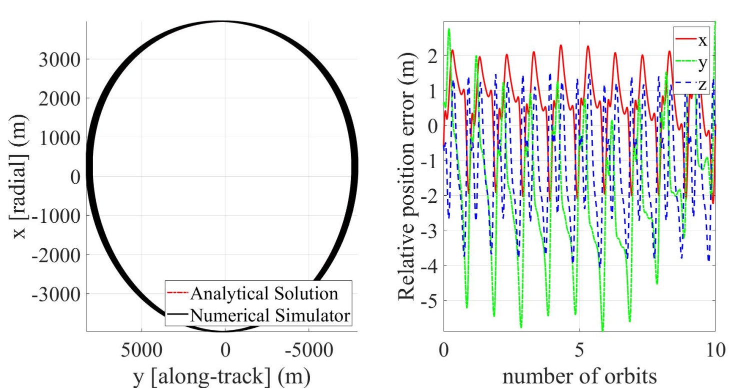

Fig. 4 Alouette-2: Previous Solution

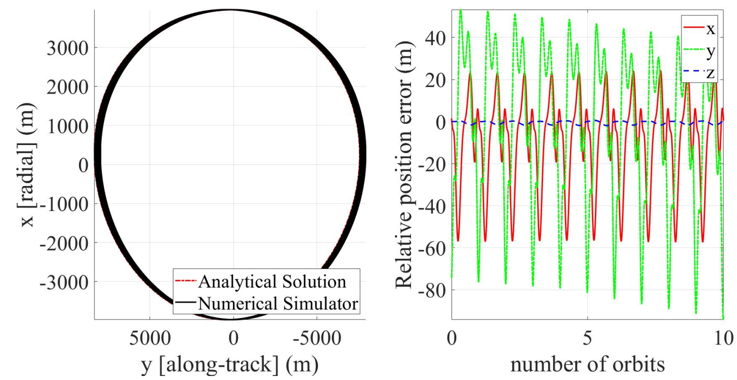

Fig. 5 Alouette-2: STM, Varying Target Orbital Elements

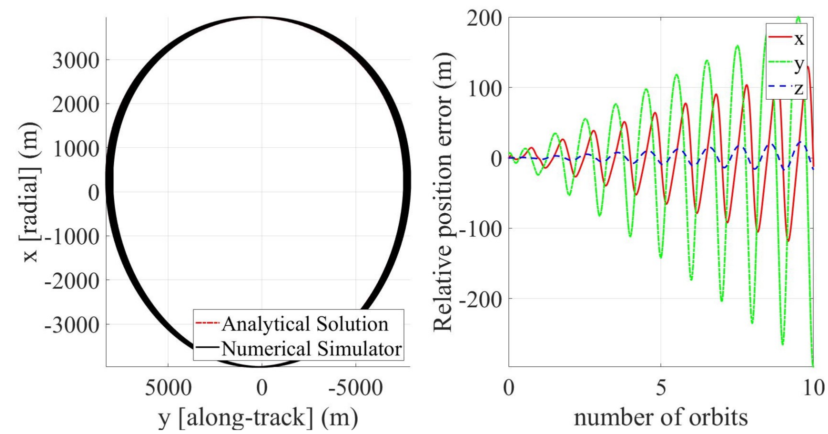

Fig. 6 Alouette-2: STM, Invariant Target Orbital Elements

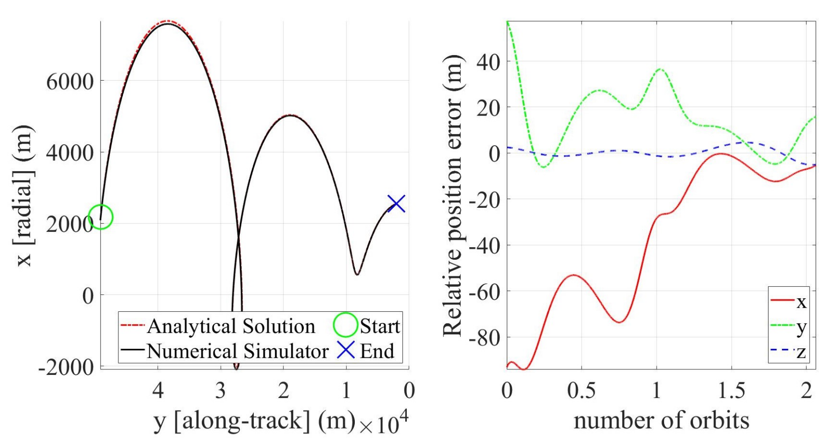

Fig. 7 Alouette-2: $\Delta t = 2T$

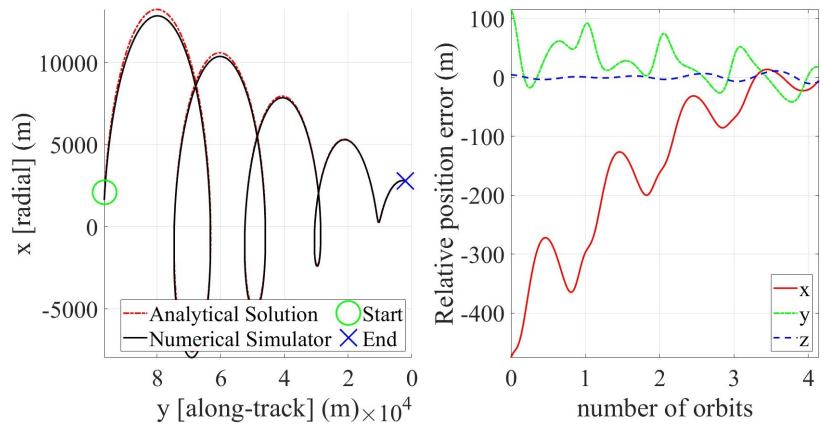

Fig. 8 Alouette-2: $\Delta t = 4T$

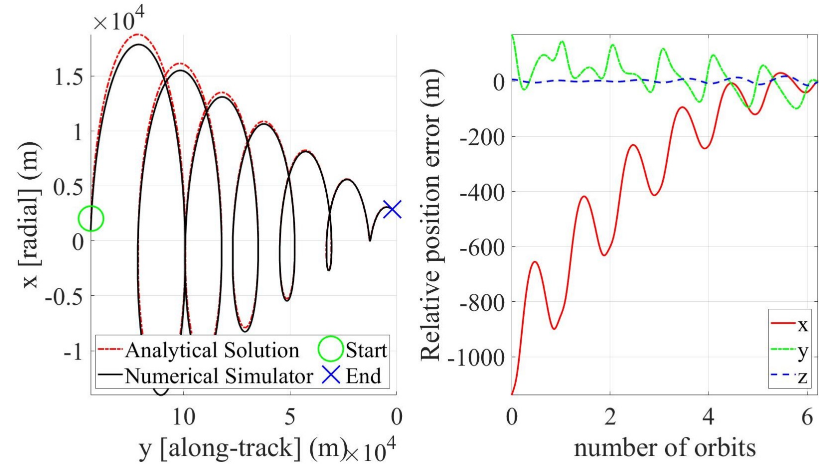

Fig. 9 Alouette-2: $\Delta t = 6T$

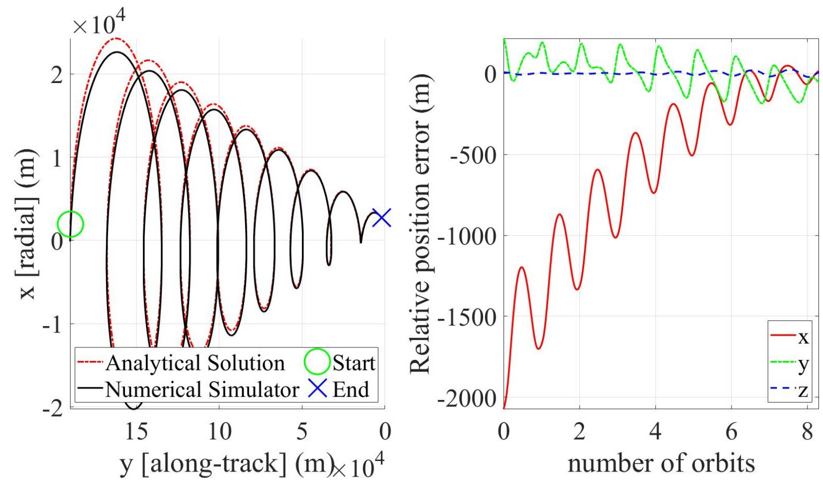

Fig. 10 Alouette-2: $\Delta t = 8T$

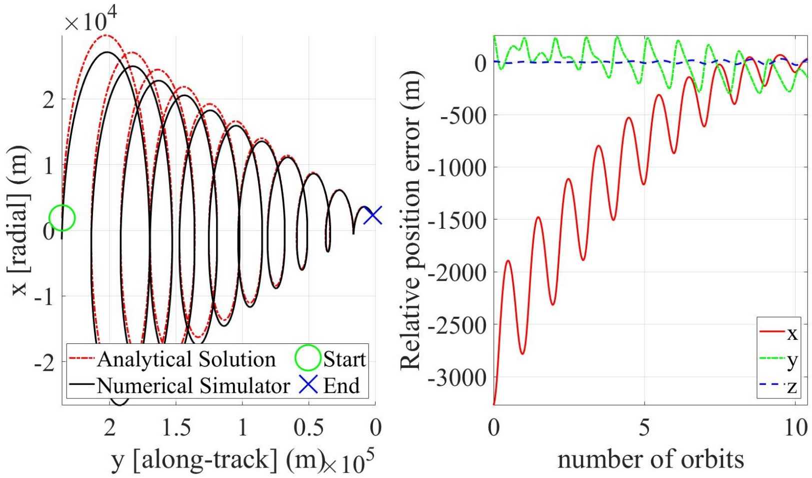

Fig. 11 Alouette-2: $\Delta t = 10T$

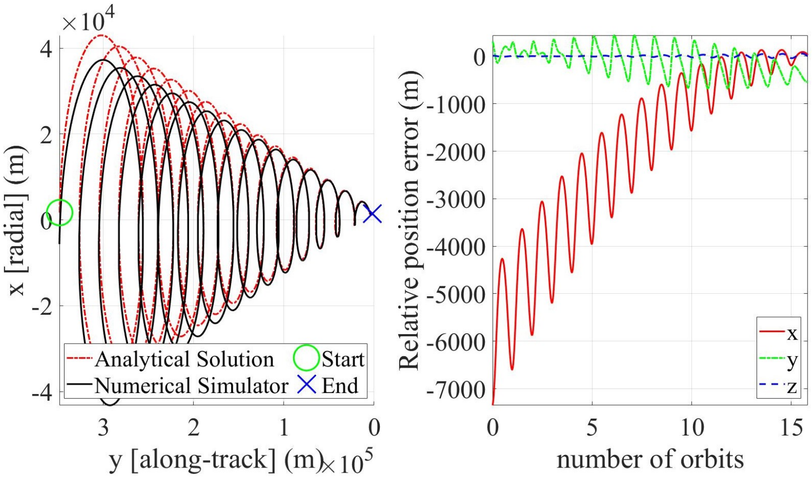

Fig. 12 Alouette-2: $\Delta t = 15T$

and Kholshevnikov's non-linear equations of motion to calculate relative motion. Additionally, the previous method employed the conversion of mean to osculating elements at every time-step whereas the new solution does not. The application of the STM in the back-propagation guidance law allows for the computation of initial relative orbital elements such that the chaser spacecraft passively drifts into the desired position with a single step. While the solution maintains an accurate tracking performance for the back-propagation guidance law, the main discrepancies lie within the desired time for which the cause is not yet known. Future work will be to include the effects of short and long periodic variations within the state-transition matrix formulation.

References

[1] Curtis, S., "The Magnetospheric Multiscale Mission... Resolving Fundamental Processes in Space Plasmas," *Report of the NASA Science and Technology Definition Team for the MMS Mission*, 2005.

[2] Peters, T. V., Branco, J., Escorial, D., Castellani, L. T., and Cropp, A., "Mission Analysis for PROBA-3 Nominal Operations," *Acta Astronautica*, Vol. 102, 2014, pp. 296–310. doi:10.1016/j.actaastro.2014.01.010.

[3] Clohessy, W. H., and Wiltshire, R. S., "Terminal Guidance System for Satellite Rendezvous," *Journal of the Aerospace Sciences*, Vol. 27, No. 9, 1960, pp. 653–658. doi:10.2514/8.8704.

[4] Ulrich, S., "Orbital Mechanics," *Carleton University, AERO 3240: Orbital Mechanics Course*, 2017.

[5] Inalhan, G., Tillerson, M., and How, J., "Relative Dynamics and Control of Spacecraft Formations in Eccentric Orbits," *Journal of Guidance, Control, and Dynamics*, Vol. 25, No. 1, 2002, pp. 48–59. doi:10.2514/2.4874.

[6] Hill, G., "Researches in the Lunar Theory," *American Journal of Mathematics*, Vol. 1, 1878, pp. 5–26.

[7] Gurfil, P., and Kholshevnikov, K. V., "Manifolds and Metrics in the Relative Spacecraft Motion Problem," *Journal of Guidance, Control, and Dynamics*, Vol. 29, No. 4, 2006, pp. 1004–1010. doi:10.2514/1.15531.

[8] Gurfil, P., and Kholshevnikov, K. V., "Distances on the Relative Spacecraft Motion Manifold," *AIAA Guidance, Navigation and Control Conference and Exhibit*, San Francisco, CA, 2005. AIAA paper 2005-5859.

[9] Gurfil, P., and Kasdin, N. J., "Nonlinear Modeling of Spacecraft Relative Motion in the Configuration Space," *Journal of Guidance, Control, and Dynamics*, Vol. 27, No. 1, 2004, pp. 154–157. doi:10.2514/1.9343.

[10] Schaub, H., "Incorporating Secular Drifts into the Orbit Element Difference Description of Relative Orbit," *Advances in the Astronautical Science*, Vol. 114, 2003, pp. 239–258.

[11] Schaub, H., and Junkins, J. L., *Analytical Mechanics of Space Systems*, AIAA American Institute of Aeronautics & Astronautics, 2018, pp. 593-673.

[12] Mahajan, B., Vadali, S. R., and Alfriend, K. T., "State-Transition Matrix for Satellite Relative Motion in the Presence of Gravitational Perturbations," *Journal of Guidance, Control, and Dynamics*, 2019, pp. 1–17. doi:10.2514/1.G004133.

[13] Guffanti, T., D'Amico, S., and Lavagna, M., "Long-term Analytical Propagation of Satellite Relative Motion in Perturbed Orbits," *AAS Spaceflight Mechanics Proceedings*, Vol. 160, 2017.

[14] Prado, A. F. B. A., "Third-body Perturbation in Orbits Around Natural Satellites," *Journal of Guidance, Control, and Dynamics*, Vol. 26, No. 1, 2003, pp. 33–40. doi:10.1155/2008/763654.

[15] Domingos, R. C., deMoraes, R. V., and Prado, A. F. B. D. A., "Third-Body Perturbation in the Case of Elliptic Orbits for the Disturbing Bodies," *Mathematical Problems in Engineering*, Vol. 2008, 2008. doi:10.1155/2008/763654.

[16] Kozai, Y., "A New Method to Compute Lunisolar Perturbations in Satellite Motions," *Smithsonian Astrophysical Observatory*, 1973, Special Report 349, pp. 1–27.

[17] Kozai, Y., "On the Effects of the Sun and Moon upon the Motion of a Close Earth Satellite," *Smithsonian Astrophysical Observatory*, 1959, Special Report 22.

[18] Lawden, D. F., "Theory of Satellite Orbits in an Atmosphere. D. G. King-Hele. Butterworths, London. 1964. 165 pp. Diagrams. 30s." *The Journal of the Royal Aeronautical Society*, Vol. 68, No. 645, 1964, p. 639–640.

[19] Brouwer, D., "Solution of the Problem of Artificial Satellite Theory without Drag," *The Astronomical Journal*, Vol. 64, No. 1274, 1959, pp. 378–396. doi:10.1086/107958.

[20] Liu, J. J. F., “Satellite Motion about an Oblate Earth,” *AIAA Journal,*, Vol. 12, No. 11, 1974, pp. 1511–1516. doi:10.2514/3.49537.

[21] Kozai, Y., “The Gravitational Field of the Earth Derived from Motions of Three Satellites,” *The Astronomical Journal*, Vol. 66, No. 1, 1961. doi:10.1086/108349.

[22] Kuiack, B., and Ulrich, S., “Nonlinear Analytical Equations of Relative Motion on J2-Perturbed Eccentric Orbits,” *AIAA Journal of Guidance, Control, and Dynamics*, Vol. 41, No. 11, 2017, pp. 2666–2677. doi:10.2514/1.G003723.

[23] Vallado, D. A., “Fundamentals of Astrodynamics and Applications,,” *El Segundo, CA, Microcosm Press, 2nd ed*, 2001, pp. 80–81.

[24] Vinti, J. P., “Zonal Harmonic Perturbations of an Accurate Reference Orbit of an Artificial Satellite,” *Mathematics and Mathematical Physics*, Vol. 67B, No. 4, 1963.

[25] Hamel, J.-F., and Lafontaine, J. D., “Linearized Dynamics of Formation Flying Spacecraft on a J2-Perturbed Elliptical Orbit,” *Journal of Guidance, Control, and Dynamics*, Vol. 30, No. 6, 2007, pp. 1649–1658.

[26] NASA, “SPACEFLIGHT REVOLUTION: The Odyssey of Project Echo,” , Accessed: January 2019. URL `https://history.nasa.gov/SP-4308/ch6.htm`.

[27] Smith, D. E., “The Perturbation of Satellite Orbits by Extra-terrestrial Gravitation,” *Planetary and Space Science*, Vol. 9, No. 10, 1962, pp. 659–674. doi:10.1016/0032-0633(62)90125-3.

[28] Cook, G. E., “Luni-Solar Perturbations of the Orbit of an Earth Satellite,” *Geophysical Journal*, Vol. 6, No. 3, 1962, pp. 271–291. doi:10.1111/j.1365-246X.1962.tb00351.x.

[29] Kaula, W. M., “Development of the Lunar and Solar Disturbing Functions for a Close Satellite,” *The Astronomical Journal*, Vol. 67, 1962, pp. 300–303. doi:10.1086/108729.

[30] Giacaglia, G. E. O., “Lunar Perturbations of Artificial Satellites of the Earth,” *Celestial Mechanics and Dynamical Astronomy*, Vol. 9, 1972, pp. 239–267.

[31] Musen, P., Bailie, A., and Upton, E., “Development of the Lunar and Solar Perturbations in the Motion of an Artificial Satellite,” *NASA-TN D494*, 1961.

[32] Izsak, I. G., “Periodic Drag Perturbations of Artificial Satellites,” *The Astronomical Journal*, Vol. 65, No. 5, 1960, pp. 355–357.

[33] Guochang Xu, W. C., Xu Tianhe, and Yeh, T.-K., “Analytic Solution of Satellite Orbit Disturbed by Atmospheric Drag,” *Monthly Notices of the Royal Astronomical Society*, Vol. 410, No. 1, 2010, pp. 654–662.

[34] Watson, J. S., Mislretta, G. D., and Bonavito, N. L., “An Analytic Method To Account For Drag In The Vinti Satellite Theory,” *Goddard Space Flight Center, Greenbelt, Maryland*, 1974, pp. 71–92.

[35] Danielson, D. A., “Semianalytic Satellite Theory,” *Master’s Thesis, Naval Postgraduate School, Monterey, California*, 1995.

[36] Martinusi, V., Dell’Elce, L., and Kerschen, G., “First-order Analytic Propagation of Satellites in the Exponential Atmosphere of an Oblate Planet,” *Celestial Mechanics and Dynamical Astronomy*, Vol. 127, No. 4, 2017, pp. 451–476.

[37] Chihabi, Y., and Ulrich, S., “Analytical Spacecraft Formation Dynamics in Eccentric Orbits with Gravitational, Drag and Third body Perturbations,” *29th AAS/AIAA Space Flight Mechanics Meeting*, Ka’anapali, HI, 13-17 Jan, 2019.